Oriented Molecular Bridge Constructs Homogeneous Buried Interface for Perovskite Solar Cells with Efficiency Over 25.3%

Xinxin Wang, Hao Huang, Min Wang, Zhineng Lan, Peng Cui, Shuxian Du, Yingying Yang, Luyao Yan, Qiang Zhang, Shujie Qu, and Meicheng Li*

Buried interface optimization matters the efficiency improvement of planar perovskite solar cells (PSCs), and the molecular bridge is reported to be an effective approach. Herein, a molecular bridge is constructed at buried interface using 4-chloro-3-sulfamoylbenzoic acid (CSBA), and its preferred arrangement is systematically investigated. It is elucidated that the CSBA molecular is prone to be orientationally absorbed on TiO_2 surface through COOH–Ti, and then connect with perovskite through S=O–Pb, resulting in a feasible oriented molecular bridge. Contributing to the passivated interfacial defects, optimized interfacial energy level, and released perovskite tensile stress, resulting from the oriented CSBA molecular bridge, the PSCs with an active area of 0.08 cm^2 achieve a certified power conversion efficiency (PCE) of 25.32%, the highest among the TiO_2-based planar PSCs. Encouragingly, the PSCs with an active area of 1 cm^2 achieve a champion PCE of 24.20%, significantly promoting the efficiency progress of large-area PSCs. In addition, the PSCs with oriented CSBA molecular bridge possess enhanced stability, the unencapsulated PSCs can maintain ≈91% and ≈85% of their initial PCE after 3000 h aging under ambient condition and 1200 h aging under exposure to UV irradiation.

1. Introduction

Metal-halide perovskite solar cells (PSCs) have attracted tremendous attention because of their high efficiency and low-cost solution preparation.[1–3] The certified power conversion efficiency (PCE) of PSCs has reached to 26.1% in 2023.[4] The theoretical PCE of PSCs is reported to be 31%, which indicates the PSCs desire more effort to approach the Shockley–Queisser (S–Q) limit.[5,6] The losses of carrier recombination at the interface

within PSCs is a key factor that limits the efficiency improvement, which makes the interfacial engineering strategy to be a feasible pathway to pursue higher PCE.[7,8]

As a typical layer-by-layer device configuration, the n-i-p PSCs have multiple interfaces including the buried interface (electron transport layer (ETL)/perovskite) and the upper interface (perovskite/hole transport layer). Under unremitting efforts over the past years, researchers have made a lot of progress in optimizing the upper interface to improve efficiency. As early as 2018, Jiang et al. adopted phenethylammonium iodide (PEAI) to passivate defects at the upper interface, achieving a certified efficiency of 23.32%, the highest PCE at that time.[9] Based on PEAI passivation, a series of passivation strategies at the upper interface using similar organic ammonium salt have been proposed, leading to the unprecedented PCE rise.[10–13] So far, researchers have gained a deep insight into the upper interface optimization, and the upper interface post-treatment has become an indispensable technology of high-efficiency PSCs fabrication. However, compared with the upper interface, the buried interface that directly affects the perovskite crystallization and interfacial charge transport has a more crucial influence on the PSCs' performance.[14] Considering the buried interface is covered and difficult to characterize, the modification progress is relatively lagging, desiring more exploration and efforts.

To date, in order to optimize the buried interface, strategies such as buffer layer, additive engineering and molecular bridge have been reported.[15–17] Among them, molecular bridge has been proven to be an effective approach to improve PSCs performance, due to its synergetic effects in manipulating interfacial carrier transport and perovskite crystallization. Chen and coworkers utilized 3-amino-4-pyrazolecarboxylic acid (denoted as APA) to construct a molecular bridge, passivating the interfacial defect and enhancing the carrier transport. Benefiting from the synergistic effect of APA, the corresponding PSCs achieve a PCE of 24.71% with a minimum open circuit voltage (V_{OC}) deficit of 0.36 V.[18] Xu et al. employed 3-sulphonato-propyl acrylate potassium salt (SPA) as a molecular bridge at TiO_2/perovskite interface, which facilitates the energetic alignment and electron

X. Wang, H. Huang, M. Wang, Z. Lan, P. Cui, S. Du, Y. Yang, L. Yan, Q. Zhang, S. Qu, M. Li
State Key Laboratory of Alternate Electrical Power System with Renewable Energy Sources
School of New Energy
North China Electric Power University
Beijing 102206, China
E-mail: mcli@ncepu.edu.cn

**ADVANCED
SCIENCE NEWS**

www.advancedsciencenews.com

**ADVANCED
MATERIALS**

www.advmat.de

extraction, resulting in the CsPbI$_3$-based PSCs deliver a PCE of 20.98% with a V_{OC} of 1.229 V.[19] When trying to construct the molecular bridge, it is the key part that selecting the suitable organic molecular. Considering that both the ETL (TiO$_2$, SnO$_2$, ZnO, and so on) and perovskite include metal atoms, researchers usually choose the molecules that include multiple coordination groups (tartaric acid, SPA, APA, etc.) to connect metal atoms located in the ETL and perovskite, respectively.[20] Although multiple molecules have been selected to construct molecular bridge, the issue of molecular arrange orientation at the buried interface has been hardly concerned and the oriented arrangement is difficult to be determined. APA, SPA, and the α-cyano-4-hydroxycinnamic acid (CHCA) have been utilized to construct the molecular bridge at buried interface, achieving an effective performance increment. However, in these works, the molecular orientation at the buried interface is proposed to be disoriented from the diagram schematic in the manuscript. The oriented molecular bridge is supposed to improve the energy order at the heterointerface and distribute a homogeneous environment.[21,22] Thus, constructing an oriented molecular bridge is expected to maximize the potential of interface bridge strategy in improving the PSCs efficiency.

Herein, we constructed an oriented molecular bridge at the TiO$_2$/perovskite buried interface, resulting in TiO$_2$-based PSCs possessing an impressive performance. We utilized 4-chloro-3-sulfamoylbenzoic acid (CSBA) as oriented molecular bridge at the buried interface. First-principles density functional theory (DFT) calculations and experimental characterizations indicate that the carboxyl group (COOH) of CSBA can preferentially connect strongly with TiO$_2$ ETL, and the sulfonyl amino group of CSBA subsequently can effectively coordinate Pb^{2+}. Due to the optimization of oriented molecular bridge on buried interface, the resultant PSCs with an active area of 0.08 and 1 cm^2 obtain champion PCE of 25.32% (certified PCE: 25.32%) and 24.20%, respectively. In addition, the TiO$_2$-CSBA based unencapsulated PSCs can maintain 91% of its initial PCE after storing in ambient conditions for 3000 hours, and the ultraviolet (UV) and operational stability have also been effectively enhanced.

2. Results and Discussion

2.1. Construction of Oriented Molecular Bridge

In order to optimize the buried interface (TiO$_2$/perovskite), we tried to construct a molecular bridge using CSBA molecule (Figure S1, Supporting Information) that contains a carboxyl group and a sulfonyl amino group. Considering the CSBA molecule is introduced on TiO$_2$ surface before the perovskite deposition, we try to demonstrate that the molecules can anchored on TiO$_2$ surface with directional arrangement at first. X-ray photoelectron spectroscopy (XPS) and energy dispersive X-ray spectroscopy (EDS) analysis were carried out to investigate the existence of CSBA and its chemical states. The high-resolution spectrum of S element of TiO$_2$-CSBA (**Figure** 1a) shows new peaks at 168.0 and 169.1 eV, undoubtedly indicating the successful introduction of CSBA on TiO$_2$. The existence of CSBA on TiO$_2$ is also verified by EDS mapping (Figure S2, Supporting Informa-

tion). The XPS spectra of the C and Ti elements are depicted in Figure 1b,c. The TiO$_2$-CSBA spectra show a new peak at 289.0 eV which represents the C=O group of CSBA.[20,23] Meanwhile, compared with the Ti 2p peaks of TiO$_2$, the Ti 2p peaks of TiO$_2$-CSBA shift 0.2 eV to lower binding energy, indicating the chemical interaction between CSBA and Ti atom. To investigate the preferred arrangement of CSBA molecule on TiO$_2$ surface, we performed DFT calculations to obtain the binding energy (E_b) of TiO$_2$ and CSBA in all possible conditions. For simplicity, we denote these adsorption systems as: mode I, mode II, mode III, and mode IV (Figure 1d). The calculated E_b values of four different adsorption systems are −0.34, −0.58, −0.56, and −1.12 eV, respectively. The smaller E_b value in mode IV indicates that CSBA molecule is prone to directional absorption on the TiO$_2$ surface through COOH-Ti. The oriented absorption structure of CSBA on TiO$_2$ is subsequently validated by Fourier-transform infrared spectroscopy (FTIR) measurement. The peak representing C=O group stretching vibration of CSBA shifts to 1591 cm^{-1} from original 1555 cm^{-1} after CSBA is absorbed on TiO$_2$ surface, which not only confirms the existence of CSBA on TiO$_2$ surface but also further proves the DFT results (Figure 1e and Figure S3, Supporting Information). Moreover, the slight variation at 912 cm^{-1} may also indicate the existence of COOH–Ti group.[23,24]

After investigating the arrangement of CSBA on TiO$_2$ surface, we further explored the preferred connecting approaches between CSBA and perovskite. We represented all possible adsorption systems of CSBA connecting perovskite as mode I, mode II, mode III, mode IV, and mode V, respectively (Figure 1f). Five E_b values calculated from different adsorption systems are −0.18, −0.35, −0.66, −0.66, and −0.74 eV, respectively. The calculated results show that the CSBA molecule is prone to connect with perovskite through sulfonyl amino group. Despite from the DFT, the liquid state nuclear magnetic resonance (NMR) was also utilized to explore the connecting approach between CSBA and perovskite. The NMR results (Figure 1g and Figure S4, Supporting Information) show that C–S peak of pure CSBA exhibits a shift from 141.39 to 141.32 ppm after incorporating into PbI$_2$, indicating the coordination between S=O and Pb^{2+}. Based on the above investigation and discussion, we can know that the CSBA is prone to be orientationally absorbed on TiO$_2$ surface through COOH–Ti, and then connects with perovskite through S=O–Pb, resulting in a feasible oriented molecular bridge at the buried interface (Figure S5, Supporting Information). This oriented molecular bridge leads to lower energy disorder and a homogeneous environment, which is supposed to enhance the interfacial carrier transport (Figure 1h and Figure S6, Supporting Information).

2.2. Interface Optimization of Oriented Molecular Bridge

2.2.1. Energy Level Matching of Buried Interface

After discussing the orientational arrangement of CSBA at buried interface, we further explore how CSBA affects the electronic properties of TiO$_2$. We collected the current density–voltage (J–V) curves of devices structured as FTO/ETLs/Au to characterize the conductivity of TiO$_2$ and TiO$_2$-CSBA. As shown in **Figure** 2a, the film conductivity can be calculated from the
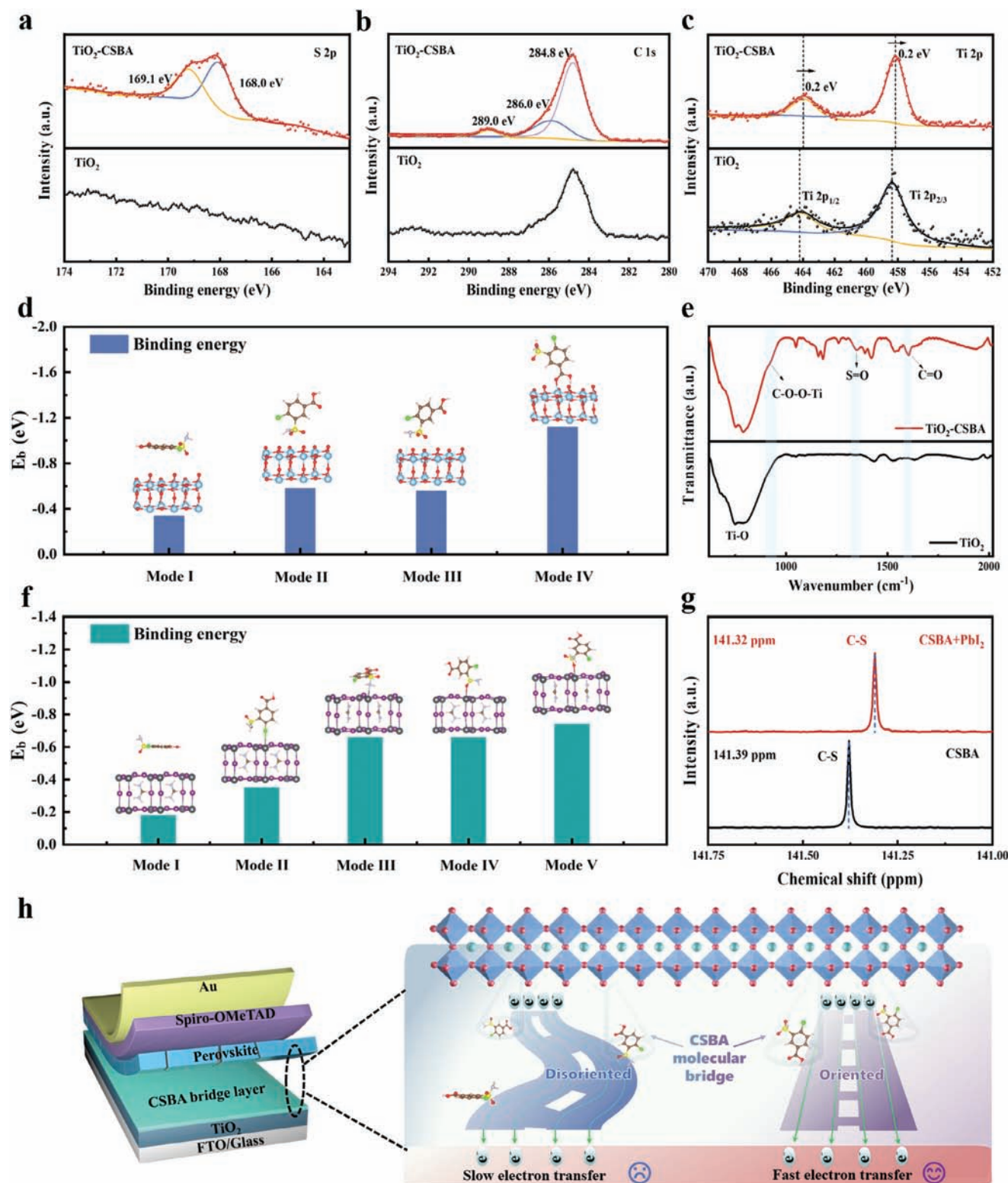
Figure 1. Oriented CSBA molecular bridge. a–c) S 2p, C 1s, and Ti 2p XPS spectra of TiO_2 and TiO_2-CSBA, respectively. d) Theoretical calculation of CSBA absorbed on TiO_2 surface. e) FTIR spectra of TiO_2 and TiO_2-CSBA. f) Theoretical calculation of CSBA absorbed on perovskite. g) ^{13}C NMR spectra of pure CSBA dissolved in DMSO-d_6 and precursor containing CSBA and PbI_2 dissolved in DMSO-d_6. h) Schematic illustration of interfacial electron transfer between perovskite and CSBA. Disoriented is left and oriented is right.

**ADVANCED
SCIENCE NEWS**

www.advancedsciencenews.com

**ADVANCED
MATERIALS**

www.advmat.de
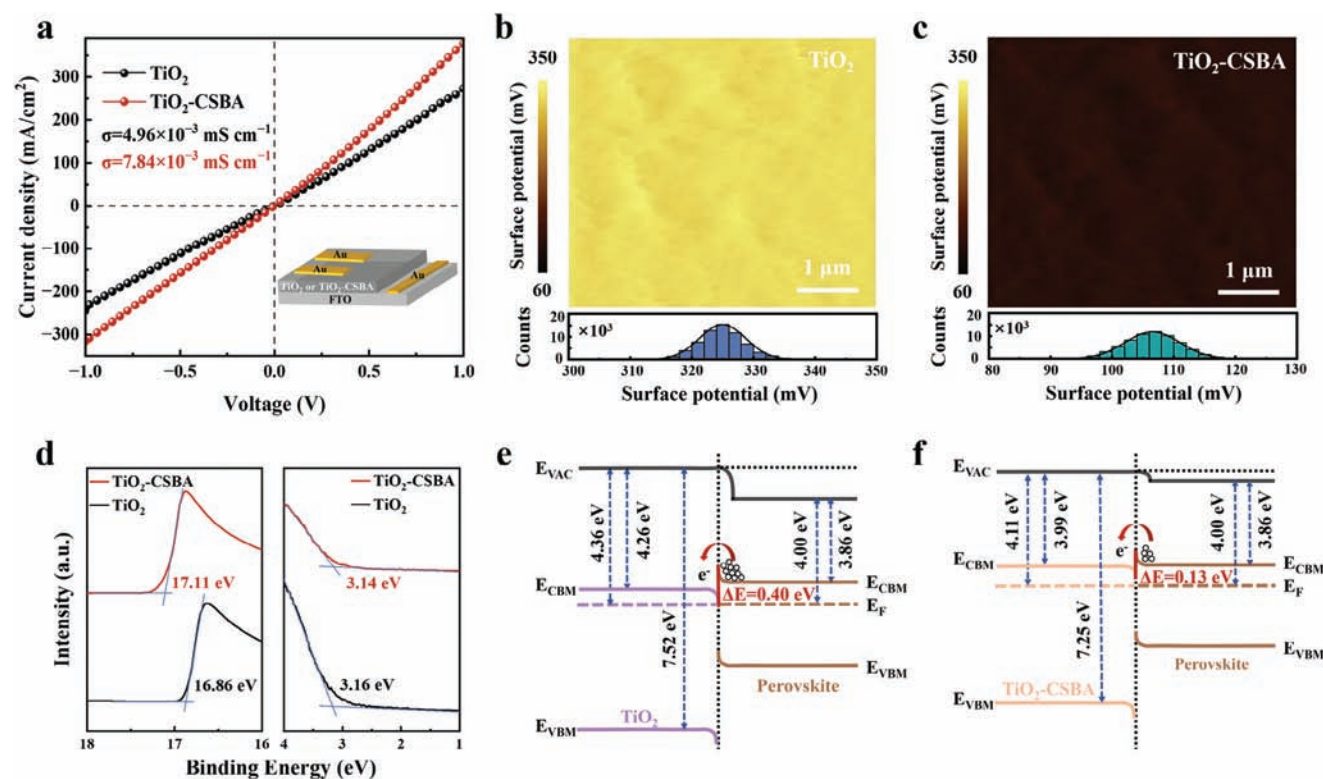
Figure 2. Characterizations of ETLs and energy band structure. a) J–V curves of devices structured as FTO/ETLs/Au. b,c) KPFM images of TiO$_2$ and TiO$_2$-CSBA. d) UPS spectra of secondary electron cut-off and valence bands of TiO$_2$ and TiO$_2$-CSBA. e,f) Energy diagram of TiO$_2$/perovskite and TiO$_2$-CSBA/perovskite.

equation of $I = \sigma A L^{-1} V$.[25] The calculated conductivity of TiO$_2$ and TiO$_2$-CSBA are 4.96×10^{-3} and 7.84×10^{-3} mS cm^{-1}, respectively. In order to investigate the energy band structure of TiO$_2$ and TiO$_2$-CSBA, we carried out measurements of kelvin probe force microscopy (KPFM), ultraviolet photoelectron spectroscopy (UPS), and UV–vis spectrophotometer. As shown in Figure 2b,c and Figure S7 (Supporting Information), the average surface potential of TiO$_2$-CSBA (106 mV) is lower than that of TiO$_2$ (324 mV), indicating an increase of the Fermi level (E_F). For obtaining more detailed information on energy level, the UPS measurement was subsequently performed on TiO$_2$ and TiO$_2$-CSBA. In Figure 2d, after the absorption of CSBA on TiO$_2$, the secondary electron cut-off ($E_{cut-off}$) edge of TiO$_2$ shifts from 16.86 to 17.11 eV, the corresponding work function value of TiO$_2$ changes from −4.36 to −4.11 eV, which is consistent with the KPFM results. Based on the obtained E_F, we further calculate the valence band maximum energy (E_{VBM}) value of TiO$_2$ to be 7.52 eV, and the E_{VBM} of TiO$_2$-CSBA to be 7.25 eV. Combining the results of Tauc plots (Figure S8a,b, Supporting Information), we also calculate the conduction band minimum energy (E_{CBM}) value of TiO$_2$ to be 4.26 eV, and the E_{CBM} of TiO$_2$-CSBA to be 3.99 eV. Based on the energy level information of ETLs and perovskite (Figure S9a,b, Supporting Information), the schematic band bending description of TiO$_2$/perovskite interface are depicted in Figure 2e,f. The energy level offset ($\Delta E = E_{CB}^{Perovskite} - E_{CB}^{TiO2}$) is reduced from 0.40 to 0.13 eV, which suggests that the oriented CSBA molecular bridge is beneficial for interfacial electron transport.

2.2.2. Strain Relaxation of Perovskite Film

Based on the above analysis, the CSBA molecular bridge can chemically bond with TiO$_2$ surface through COOH group, and coordinate with Pb^{2+} through sulfonyl amino group at buried interfaces, which may influence the perovskite crystallization. To gain an insight into the crystalline quality of perovskite film, top-view scanning electron microscopy (SEM) images were obtained to study the surface topography of perovskite films deposited on different substrates. As shown in **Figure 3a,b**, both the perovskite films are compact and pinhole-free. After constructing the oriented molecular bridge, the average size of grain in perovskite film is slightly larger. We can also notice that the perovskite crystals of perovskite film deposited on TiO$_2$-CSBA convert to monolithic grains vertical to the substrate (Figure S10a,b, Supporting Information). Besides, the atomic force microscope (AFM) was also carried out to analyze the surface morphology and grain of perovskite films (Figure S11, Supporting Information), which is consistence with the SEM results. In addition, X-ray diffraction (XRD) characterization is conducted to further analyze the crystallinity of perovskite films on different substrates. In Figure S12a (Supporting Information), two strong diffraction peaks observed at 14.14° and 24.48° belong to (100) and (111) crystal planes.[26] We normalized the peak intensity and found that the PbI$_2$/(100) peak ratio of perovskite films deposited on TiO$_2$-CSBA was significantly decreased (Figure S12b, Supporting Information), indicating that the residual PbI$_2$ of perovskite was reduced. As shown in Figure 3c, the perovskite film on TiO$_2$-
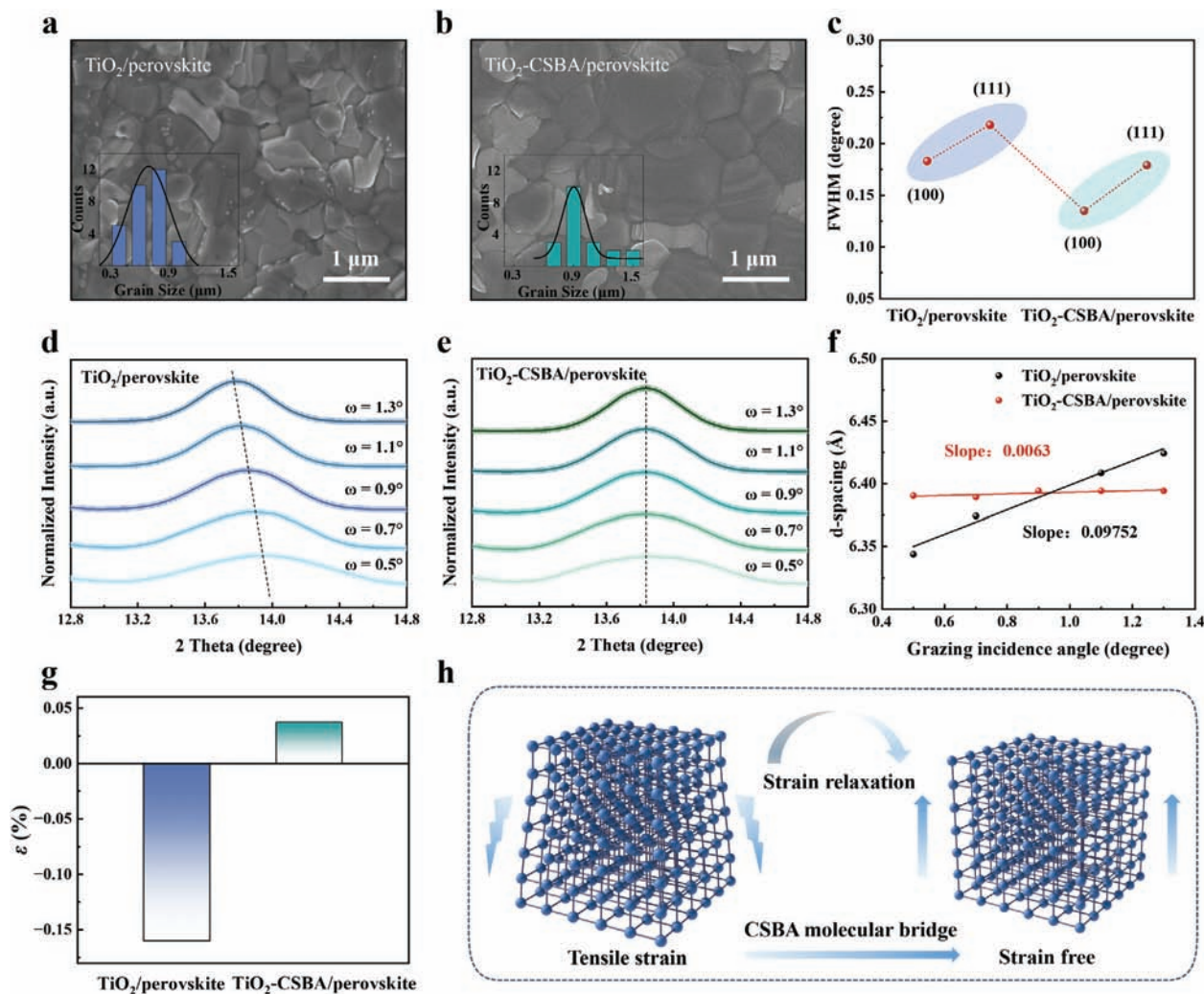
Figure 3. Strain characterization of perovskite films. a,b) Surface morphologies of perovskite films on TiO_2 and TiO_2-CSBA. c) FWHM of (100) and (111) peaks. d,e) GIXRD spectra for TiO_2-based and TiO_2-CSBA based perovskite films at different tilt angles. f) The d-spacing values obtained from (100) plane as a function of incidence angle. g) Histogram of strain (ϵ). h) Schematic diagram of residual strain.

CSBA shows smaller width at half maximum (FWHM) on both (100) and (111) planes, indicating the enhanced crystallinity.

The residual strain is commonly observed in perovskite film, which has a severe impact on PSCs efficiency and stability.[27,28] It is reported that the residual strain may come from external stimuli during PSCs preparation and the mismatch of thermal expansion coefficient at buried interface (TiO_2/perovskite film).[29–31] To investigate the residual strain present in perovskite films on both TiO_2 and TiO_2-CSBA, we employed depth-resolved grazing incidence X-ray diffraction (GIXRD) technology.[32,33] As exhibited in Figure 3d,e, by varying ω (the grazing incidence angle) from 0.5° to 1.3°, the scattering peaks of (100) plane in TiO_2-perovskite film gradually shift toward a smaller angle. According to the Bragg equation of $n\lambda = 2d\sin\theta$, the downshift of scattering peak indicates the increased crystal plane distance, which demonstrates the existence of lattice tensile strain in the perovskite film.[34] In contrast, the scattering peaks of (100) plane in TiO_2-CSBA based perovskite film exhibits almost invisible offset, indicating that there exists negligible in-plane lattice ten-

sile strain. In detail, we calculated the slopes of the corresponding fitted line of d-spacing and grazing incidence angle for both perovskite films. As shown in Figure 3f, the slope changes from 0.09752 to 0.0063 after constructing the oriented molecular bridge. These results indicate that the TiO_2-CSBA based perovskite film has released the residual tensile strain. Moreover, the lattice strain of perovskite film on TiO_2-CSBA is 3.7×10^{-4} calculated by Williamson–Hall plots, smaller than that of perovskite film on TiO_2 (1.6×10^{-3}) (Figure 3g and Figure S13, Supporting Information). The released residual strain may be ascribed to the decreased interfacial traps and improved interfacial contact resulting from oriented molecular bridge (Figure 3h).[35]

2.2.3. Interfacial Charge Transport and Device Physical Property

We now investigate the effects of oriented molecular bridge on interfacial carrier transport and device physical property. Based on the previous researches on the perovskite films

**ADVANCED
SCIENCE NEWS**

www.advancedsciencenews.com

**ADVANCED
MATERIALS**

www.advmat.de
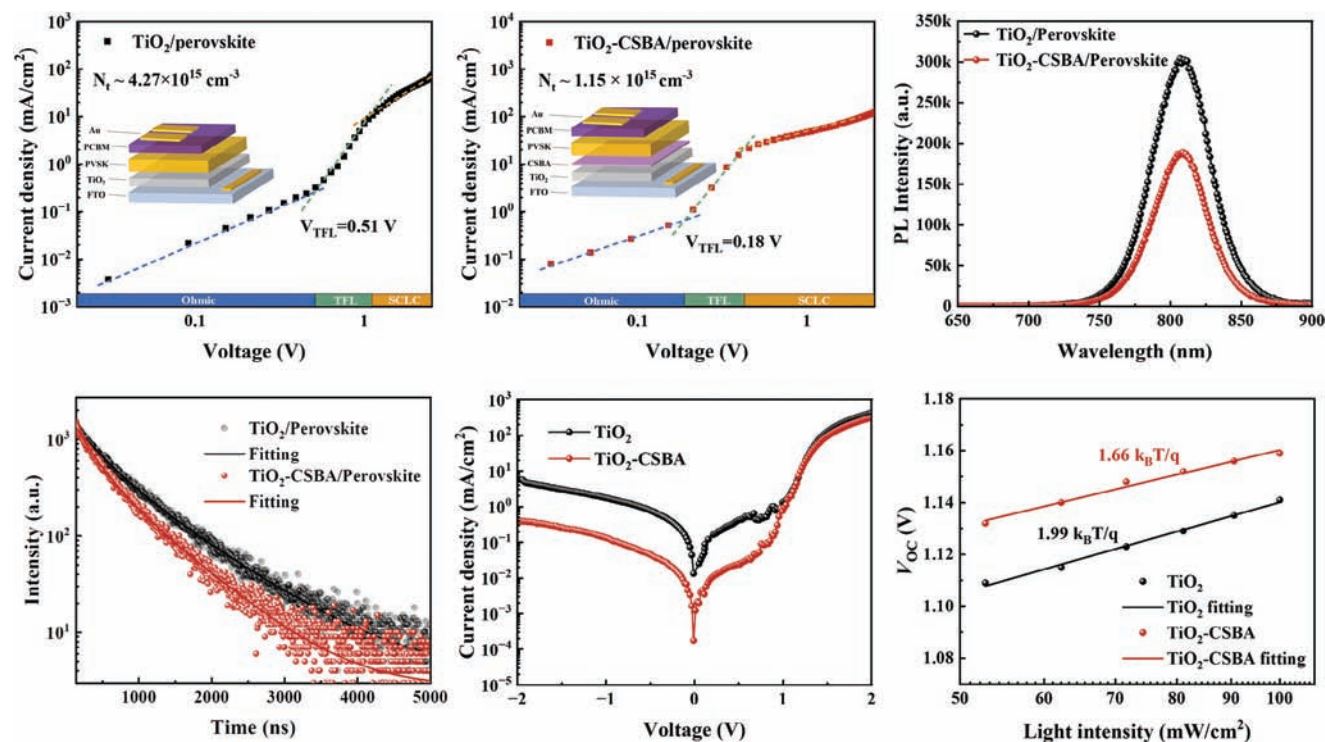
Figure 4. Characterization of device physical property. a,b) Space charge limited current curves for electron-only devices. c,d) PL and TRPL spectra of perovskite films on TiO_2 and TiO_2-CSBA. e) Dark J–V curves of TiO_2 and TiO_2-CSBA based PSCs. f) The relationship between the V_{OC} of PSCs and light intensity.

on different substrates, we further quantitatively estimated their defect density (N_t). We prepared electron-only devices (FTO/ETLs/perovskite/PCBM/Au) and performed space-charge limited current (SCLC) measurements. As depicted in **Figure 4a,b**, N_t can be calculated according to the equation of $N_t = (2\epsilon\epsilon_0 V_{TFL})/(qL^2)$.[36] The calculated N_t of perovskite film on TiO_2 is 4.27×10^{15} cm^{-3}, and the calculated N_t of perovskite film on TiO_2-CSBA is 1.15×10^{15} cm^{-3}. To further verify that CSBA molecular bridge can passivate interfacial defects, we designed an assisted experiment by spin-coating the CSBA on the upper and bottom sides of the perovskite film, and then compare their PL intensity. As shown in Figure S14 (Supporting Information), no matter whether CSBA is spin-coated on the top or bottom of the perovskite film, a significant increase in PL intensity can be observed. Besides, steady-state photoluminescence (PL) and time-resolved PL (TRPL) have been carried out to understand the influence of oriented molecular bridge on interfacial carrier transport. Compared to the spectrum of perovskite film on TiO_2, the spectrum of perovskite film on TiO_2-CSBA shows tremendous quenching of PL intensity, indicating a more effective electron extraction (Figure 4c). The TRPL curves and fitted carrier lifetime are depicted in Figure 4d and Table S1 in the Supporting Information. The TRPL curves were fitted using a biexponential decay equation. The value of τ_1 corresponding to the fast decay component is obviously reduced from 339.39 ns (TiO_2 based) to 245.48 ns (TiO_2-CSBA based), and τ_{ave} also decreases from 592.51 to 438.49 ns. These results testify the efficient electron extraction and the reduced nonradiative recombination at buried interface with the oriented molecular bridge.[36] The reason for improved

electron extraction should be attributed to optimized electronic property of ETL and the energy level match of ETL/perovskite interface.

From the perspective of device, the dark J–V curves for TiO_2 and TiO_2-CSBA based PSCs are shown in Figure 4e. The dark saturation current density (J_0) is effectively suppressed due to the defect passivation resulting from oriented molecular bridge. In addition, the relationship between V_{OC} and light intensity was explored according to the equation $V_{OC} = \frac{n_{ID}k_B T}{q} \ln(l)$ (k_B is the Boltzmann constant and q represents the elementary charge). We calculate the ideality factors (n_{ID}) to be 1.99 and 1.66 for TiO_2 and TiO_2-CSBA based PSCs, respectively (Figure 4f). The smaller n_{ID} indicates the reduced trap-assisted recombination within the PSCs. Apparently, the oriented molecular bridge can accelerate the interfacial carrier transport and inhibit nonradiative recombination within the PSCs, which is beneficial to fabricating high-efficiency PSCs.

2.3. Photovoltaic Performance of PSCs

We fabricated planar PSCs using TiO_2 or TiO_2-CSBA as ETL and collected their photovoltaic parameters. First, we explored the influence of CSBA concentration on PCE of PSCs. As shown in Figure S15 (Supporting Information), the PSCs exhibit the highest PCE when the concentration of CSBA is 1 mg mL^{-1}. Hereafter, all TiO_2-CSBA based PSCs were fabricated with the amount of CSBA being 1 mg mL^{-1}. As shown in **Figure 5a**, the TiO_2-CSBA based PSCs with 0.08 cm^2 active area exhibits a champion

ADVANCED
SCIENCE NEWS
www.advancedsciencenews.com

ADVANCED
MATERIALS
www.advmat.de
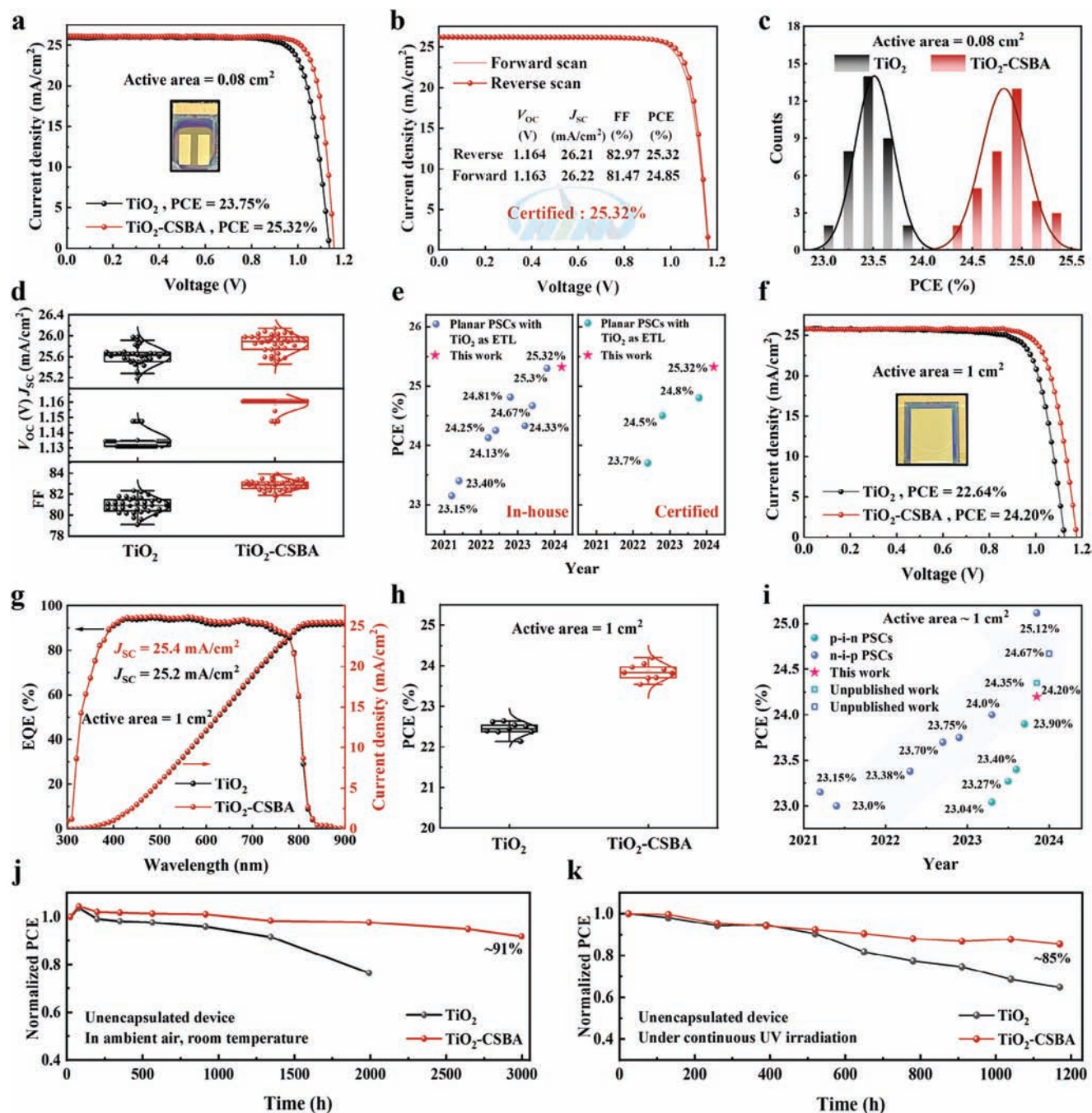
Figure 5. Photovoltaic performance and stability of TiO$_2$ and TiO$_2$-CSBA based PSCs. a) The reverse *J–V* curves of TiO$_2$ and TiO$_2$-CSBA based PSCs with active area of 0.08 cm^2. b) *J–V* curves measured at National Institute of Metrology, an independent solar cell-accredited laboratory. c,d) Distribution histograms of PCE value and detailed photovoltaic parameters statistics among 35 PSCs. e) PCE comparison of our PSC with the reported efficient PSCs. The left side shows the PCE values measured in-house and the right side shows the certified PCE values. f) The reverse *J–V* curves of TiO$_2$ and TiO$_2$-CSBA based PSCs with active area of 1 cm^2. g) The EQE spectra of TiO$_2$ and TiO$_2$-CSBA based PSCs with active area of 1 cm^2. h) PCE distribution of TiO$_2$ and TiO$_2$-CSBA based PSCs with active area of 1 cm^2. i) PCE comparison between our PSC and reported PSCs, the active area of these PSCs is near 1 cm^2. j) PCE evolution of unencapsulated TiO$_2$ and TiO$_2$-CSBA based PSCs stored under ambient air. k) PCE evolution of unencapsulated TiO$_2$ and TiO$_2$-CSBA based PSCs under continuous UV (254 nm) irradiation in N$_2$-glovebox.

PCE of 25.32%. The hysteresis of PSCs with different ETLs is shown in Figure S16 and Table S2 (Supporting Information), the hysteresis factor of TiO$_2$-CSBA based PSCs is 1.8%, which is smaller than that (2.5%) of TiO$_2$ based PSCs. Encouragingly, the best-performing TiO$_2$-CSBA based PSCs obtained a certified PCE of 25.32%, breaking the efficiency record of TiO$_2$-based planar PSCs to date (Figure 5b and Figure S17, Supporting Information). The corresponding external quantum efficiency (EQE) spectra are shown in Figure S18 (Supporting Information), the TiO$_2$-CSBA based PSCs present an integrated J_{SC} of 25.6 mA cm^{-2} with a small variation from the values shown in Figure 5a. The statistic distributions of photovoltaic parameters are presented in Figure 5c,d, TiO$_2$-CSBA based PSCs show excellent reproducibility with a larger average PCE of 24.8% than that (PCE$_{ave}$ = 23.7%) of TiO$_2$ based PSCs. It is worth noting that we made a comprehensive efficiency comparison of TiO$_2$-based planar PSCs between our work and reported works. As shown in Figure 5e and Table S3 (Supporting Information), we can find that the certified PCE of 25.32% achieved in our work is apparently much higher than the others in reported works, which demonstrates the positive effect of oriented molecular bridge on improving the PSCs efficiency.

Besides, we also fabricated PSCs with an active area of 1 cm^2 (Figure 5f and Table S4, Supporting Information). The TiO$_2$-CSBA based PSCs achieve a champion PCE of 24.20% which is much higher than that (22.64%) of TiO$_2$-based PSCs. The authenticity of J_{SC} is confirmed by the EQE measurements (Figure 5g) and the repeatability was also confirmed by statistic distributions of 10 PSCs Figure 5h,i shows the PCE comparisons of PSCs with an active area of 1cm^2 between our work and the reported works, it can be found that the 24.20% achieved in this work is superior to most reported values (Table S5, Supporting Information), promoting the performance progress of large-area PSCs.

Except from confirming the positive effect of oriented molecular bridge on efficiency, we also explored its effect on PSCs stability. In order to characterize the PSCs stability under ambient condition (25 °C and 10% relative humidity (RH)), first, the PCE evolution of unencapsulated PSCs after aging for 3000 h was monitored. As shown in Figure 5j, the TiO$_2$-CSBA based PSCs can maintain ≈91% of their initial efficiency, while the TiO$_2$ based PSCs can only maintain ≈76% in no more than 2000 h. Second, to investigate the stability of TiO$_2$ based PSCs under ultraviolet (UV) irradiation, these PSCs were continuously irradiated by UV lamp ($\lambda = 254$ nm) under N$_2$ environment (according to the previous work, the temperature of PSCs during the UV irradiation test was ≈45 °C).[20] As displayed in Figure 5k, after 1200 h of UV radiation, the TiO$_2$ and TiO$_2$-CSBA based PSCs can maintain ≈62% and ≈85% of their initial values, respectively. The distinctly enhanced stability against UV light may be attributed to the release lattice strain and reduced defects, which alleviate degradation of perovskite induced by light stress.[37] Finally, the operational stability was further investigated through tracking the power output when the PSCs were continuously light soaked (white LED, 100 mW cm^{-2}) in the N$_2$-glove box. The TiO$_2$-CSBA based PSCs can maintain 92% of the original PCE after operating for 140 h, while the TiO$_2$ based PSCs declined to 77% of their initial value (Figure S19, Supporting Information). High temperature and high humidity are also needed to be considered when evaluating the stability of PSCs. We carried out the stability test at

harsh condition (85% RH, 85 °C, double 85 (85% RH and 85 °C). It is found that the oriented molecular bridge can effectively improve the device photovoltaic performance and also possess a positive effect on the stability (Figure S20 and Note S1, Supporting Information). Overall, the reduced interfacial defects, the optimized perovskite film and the release lattice strain are account for the remarkable photovoltaic performance and better stability.

3. Conclusion

In summary, we have realized high-efficiency planar PSCs by constructing an oriented CSBA molecule bridge at buried TiO$_2$/perovskite interface. Owing to the passivated interfacial defects, enhanced electron extraction and released tensile stress of perovskite film, the PSCs (active area of 0.08 cm^2) obtain a certified PCE of 25.32%, the highest among the TiO$_2$-based planar PSCs reported so far. Notably, the large-area TiO$_2$-CSBA based PSCs with active area of 1 cm^2 achieved a champion PCE of 24.20%. In addition, the nonencapsulated TiO$_2$-CSBA based PSCs possess excellent long-term stability, which can maintain ≈91% and ≈85% of their initial PCE after aging under ambient conditions for 3000 h and UV radiation for 1200 h, respectively. We proposed that when trying to constructing an oriented molecular bridge, the functional groups, the molecular configuration and the molecule size should be fully considered. We believe that our strategy of oriented molecular bridge and the insight of molecular preferred arrangement provide guidelines for solving bottleneck issues regarding the buried interface, and more opportunity to achieve high performance and stable PSCs.

4. Experimental Section

Materials and Reagents: FTO Glass (7 Ω sq^{-1}) was purchased from Shangyang Solar Energy Technology CO., Ltd. (Suzhou, China). Materials required for preparing TiO$_2$ and TiO$_2$-CSBA electron transport layer: titanium tetrachloride (purity: 99.99%) precursor and 4-chloro-3-sulfamoylbenzoic acid were purchased from Aladdin (Shanghai, China). Materials required for fabricating perovskite layer: lead iodide (purity: 99.999%) was purchased from Tokyo Chemical Industry (TCI). Rubidium chloride (RbCl) was purchased from Sigma Aldrich. Formamidinium iodide (FAI), methylammonium chloride (MACl) were purchased from Xi'an Yuri Solar CO., Ltd. N, N-dimethylformamide (DMF), dimethyl sulfoxide (DMSO), acetonitrile (ACN), chlorobenzene (CB), and isopropanol (IPA) were purchased from Sigma–Aldrich. Materials required for fabricating Spiro-OMeTAD hole transport layer: tert-butylpyridine (tBP), li-bis(trifluoromethanesulfonyl)imid (Li-TFSI), 2,2',7,7'-tetrakis (N, N-dipmethoxyphenylamine)−9,9'spirobifluorene (spiro-OMeTAD), were purchased from Xi'an Yuri Solar CO., Ltd.

Device Fabrication: The patterned F-doped tin oxide (FTO) glass (7 Ω sq^{-1}) was sequentially ultrasonic cleaned with detergent (2 vol%), deionized (DI) water, ethanol, and DI water for 15–20 min, respectively. After drying the FTO substrate with N$_2$ stream, the substrates were treated by UVO illuminated for 20 min before fabricated TiO$_2$ ETL. TiO$_2$ solution was prepared according to this previous work,[20] TiCl$_4$ precursor (4 mL) and DI water (200 mL) were mixed, then stir it up. The compact TiO$_2$ layer were fabricated by immersing FTO in 200 mL mixed solution at 70 °C for 40 min. For fabricating TiO$_2$-CSBA substrates, CSBA solution was first prepared by dissolving 1 mg CSBA powder in 1 mL methanol. Subsequently, 65 µL CSBA solution was dropped on the surface of TiO$_2$ then spin-coated at 4500 rpm for 30 s. The sample was annealed at 100 °C for 5 min after spin-coating. Then, the TiO$_2$-CSBA was washed by DMF solvent for removing the uncoordinated CSBA molecular. The perovskite

films were fabricated by a two-step deposition method according to recent report.[38] The 1.5 м PbI_2 with 3% molar RbCl was dissolved in a mixed solvent of DMF/DMSO (volume ratio 9:1). The precursor was spin-coated on FTO/ETLs at 1500 rpm for 30 s and then annealed at 70 °C for 1 min. After the PbI_2 film cooled down, the amines salts solution (90 mg FAI and 13 mg MACl dissolved in 1 mL IPA) was spin-coated on as-prepared PbI_2 film at 1800 rpm for 30 s. The perovskite precursor films were immediately taken out of the N_2-glovebox and then annealed at 150 °C for 15 min in air conditions (relative humidity between 30% and 40%). The annealed substrates then transferred back into N_2-glovebox. The MeO-PEAI solution (4.5 mg in 1 mL IPA) was spin-coated on fabricated perovskite film at 4500 rpm for 30 s. The Spiro-OMeTAD solution containing 72.3 mg spiro-MeOTAD, 26.6 µL tBP, and 18 µL Li-TFSI (520 mg mL^{-1} in ACN) was spin-coating at 4000 rpm for 30 s on the top of MeO-PEAI layer. At last, 80 nm Au electrode was thermal-evaporated on the top to obtain the PSCs.

Characterization: XPS and UPS were measured by ESCALAB 250Xi system equipped (Thermo Fisher Scientific). The SEM morphologies and EDS mapping images were examined using HITACHI SU8010. FTIR spectra of CSBA, TiO_2, and TiO_2-CSBA were characterized with Bruker INVENIO using attenuated total reflection (ATR) mode. The KPFM results of TiO_2 and TiO_2-CSBA were obtained using an atomic force microscope (FM-Nanoview 1000). The UV–vis spectra were recorded on a SHIMADZU, UV-2600 spectrometer. ^{13}C NMR spectra were characterized by Ascend 600 (Bruker Co., Germany). The XRD patterns of the perovskite films deposited on TiO_2 and TiO_2-CSBA were obtained on an X-ray diffractometer (D8 Advance, Bruker). The GIXRD measurement was carried out by Micromax-007HF equipment. Steady-state PL and time-resolved PL were performed by a FLS980 spectrometer (Edinburgh Instrument). The current–voltage (*J–V*) characteristics of PSCs was measured using a Keithley 2400 Source Meter with a power density of 100 mW cm^{-2}. The external quantum efficiency (EQE) spectra of PSCs were achieved using a QE-R system (Enli Tech.).

DFT Calculations: All calculations were used the Vienna ab initio simulation package (VASP),[39,40] and the exchange–correlation energy have been treated using the Perdew–Burke–Ernzerhof (PBE) function.[41] Van der Waals forces were taken into account in the calculations.[42] The cutoff energy was set up of 520 eV and the energy and force convergence parameters were set to 10^{-5} eV and 0.05 eV Å^{-1}, respectively. The binding energies of CSBA molecules on TiO_2 (101) or α-$FAPbI_3$ (100) surfaces were calculated to investigate their interactions. The TiO_2 surface model and the $FAPbI_3$ surface model were constructed from 3 × 4 supercells of TiO_2 (101) and 2 × 2 supercells of α-$FAPbI_3$ (100), respectively. To avoid interactions between adjacent slabs, a vacuum layer of more than 20 Å was added to the surface in the 2D slab model. The binding energy (E_b)[43] is based on the following equation

$$E_b = E_{molecule-slab} - E_{molecule} - E_{slab} \qquad (1)$$

Where $E_{molecule-slab}$, $E_{molecule}$, E_{slab} are the energy of the molecules adsorbed on the surface, individual molecules, and the clean TiO_2 or α-$FAPbI_3$ surface, respectively.

Supporting Information

Supporting Information is available from the Wiley Online Library or from the author.

Conflict of Interest

The authors declare no conflict of interest.

Data Availability Statement

The data that support the findings of this study are available from the corresponding author upon reasonable request.

[1] P. Cui, D. Wei, J. Ji, H. Huang, E. Jia, S. Dou, T. Wang, W. Wang, M. Li, *Nat. Energy* **2019**, *4*, 150.

[2] K. Xiao, J. Wen, Q. Han, R. Lin, Y. Gao, S. Gu, Y. Zang, Y. Nie, J. Zhu, J. Xu, H. Tan, *ACS Energy Lett.* **2020**, *5*, 2819.

[3] L. Yan, H. Huang, P. Cui, S. Du, Z. Lan, Y. Yang, S. Qu, X. Wang, Q. Zhang, B. Liu, X. Yue, X. Zhao, Y. Li, H. Li, J. Ji, M. Li, *Nat. Energy* **2023**, *8*, 1158.

[4] National Renewable Energy Laboratory, *Best Research-Cell Efficiency Chart* **2023**, https://www.nrel.gov/pv/cell-efficiency.html (accessed: December 2023).

[5] W. Shockley, H. J. Queisser, *J. Appl. Phys.* **1961**, *32*, 510.

[6] S. Rühle, *Sol. Energy* **2016**, *130*, 139.

[7] Z.-W. Gao, Y. Wang, W. C. H. Choy, *Adv. Energy Mater.* **2022**, *12*, 2104030.

[8] K. Park, J.-H. Lee, J.-W. Lee, *ACS Energy Lett.* **2022**, *7*, 1230.

[9] Q. Jiang, Y. Zhao, X. Zhang, X. Yang, Y. Chen, Z. Chu, Q. Ye, X. Li, Z. Yin, J. You, *Nat Photonics* **2019**, *13*, 460.

[10] Q. Cao, T. Wang, J. Yang, Y. Zhang, Y. Li, X. Pu, J. Zhao, H. Chen, X. Li, I. Tojiboyev, J. Chen, L. Etgar, X. Li, *Adv. Funct. Mater.* **2022**, *32*, 2201036.

[11] J. Zhou, M. Li, S. Wang, L. Tan, Y. Liu, C. Jiang, X. Zhao, L. Ding, C. Yi, *Nano Energy* **2022**, *95*, 107036.

[12] T. Li, J. Xu, R. Lin, S. Teale, H. Li, Z. Liu, C. Duan, Q. Zhao, K. Xiao, P. Wu, B. Chen, S. Jiang, S. Xiong, H. Luo, S. Wan, L. Li, Q. Bao, Y. Tian, X. Gao, J. Xie, E. H. Sargent, H. Tan, *Nat. Energy* **2023**, *8*, 610.

[13] S. Tan, T. Huang, I. Yavuz, R. Wang, T. W. Yoon, M. Xu, Q. Xing, K. Park, D.-K. Lee, C.-H. Chen, R. Zheng, T. Yoon, Y. Zhao, H.-C. Wang, D. Meng, J. Xue, Y. J. Song, X. Pan, N.-G. Park, J.-W. Lee, Y. Yang, *Nature* **2022**, *605*, 268.

[14] Y. Zhang, Y. Wang, L. Zhao, X. Yang, C.-H. Hou, J. Wu, R. Su, S. Jia, J.-J. Shyue, D. Luo, P. Chen, M. Yu, Q. Li, L. Li, Q. Gong, R. Zhu, *Energy Environ. Sci.* **2021**, *14*, 6526.

[15] Y. Ge, F. Ye, M. Xiao, H. Wang, C. Wang, J. Liang, X. Hu, H. Guan, H. Cui, W. Ke, C. Tao, G. Fang, *Adv. Energy Mater.* **2022**, *12*, 2200361.

[16] L. Yang, J. Feng, Z. Liu, Y. Duan, S. Zhan, S. Yang, K. He, Y. Li, Y. Zhou, N. Yuan, J. Ding, S. F. Liu, *Adv. Mater.* **2022**, *34*, 2201681.

[17] Z. Liu, K. Deng, J. Hu, L. Li, *Angew. Chem.* **2019**, *131*, 11621.

[18] Y. Chen, Q. Wang, W. Tang, W. Qiu, Y. Wu, Q. Peng, *Nano Energy* **2023**, *107*, 108154.

[19] C. Xu, S. Zhang, W. Fan, F. Cheng, H. Sun, Z. Kang, Y. Zhang, *Adv. Mater.* **2023**, *35*, 2207172.

[20] H. Huang, P. Cui, Y. Chen, L. Yan, X. Yue, S. Qu, X. Wang, S. Du, B. Liu, Q. Zhang, Z. Lan, Y. Yang, J. Ji, X. Zhao, Y. Li, X. Wang, X. Ding, M. Li, *Joule* **2022**, *6*, 2186.

[21] Y. Jiang, J. Wang, H. Zai, D. Ni, J. Wang, P. Xue, N. Li, B. Jia, H. Lu, Y. Zhang, F. Wang, Z. Guo, Z. Bi, H. Xie, Q. Wang, W. Ma, Y. Tu, H. Zhou, X. Zhan, *J. Am. Chem. Soc.* **2022**, *144*, 5400.

[22] C.-M. Hung, C.-L. Mai, C.-C. Wu, B.-H. Chen, C.-H. Lu, C.-C. Chu, M.-C. Wang, S.-D. Yang, H.-C. Chen, C.-Y. Yeh, P.-T. Chou, *Angew. Chem.* **2023**, *62*, 202309831.

[23] R. Djellabi, B. Yang, Y. Wang, X. Cui, X. Zhao, *Chem. Eng. J.* **2019**, *366*, 172.

[24] P. V. Bakre, S. G. Tilve, *ChemistrySelect* **2017**, *2*, 7063.

[25] Y. Ai, Y. Zhang, J. Song, T. Kong, Y. Li, H. Xie, D. Bi, *J. Phys. Chem. Lett.* **2021**, *12*, 10567.

[26] L. Shen, P. Song, L. Zheng, K. Liu, K. Lin, W. Tian, Y. Luo, C. Tian, L. Xie, Z. Wei, *J. Mater. Chem. A* **2021**, *9*, 20807.

[27] J. Zhao, Y. Deng, H. Wei, X. Zheng, Z. Yu, Y. Shao, J. E. Shield, J. Huang, *Sci. Adv.* **2017**, *3*, eaao5616.

[28] N. Rolston, K. A. Bush, A. D. Printz, A. Gold-Parker, Y. Ding, M. F. Toney, M. D. Mcgehee, R. H. Dauskardt, *Adv. Energy Mater.* **2018**, *8*, 1802139.

[29] A. Namvar, M. Dehghany, S. Sohrabpour, R. Naghdabadi, *Sol. Energy* **2016**, *135*, 366.

[30] S. Hubbard, C. Cress, C. Bailey, R. Raffaelle, S. Bailey, D. Wilt, *Appl. Phys. Lett.* **2008**, *92*, 123512.

[31] S. M. Lee, D. H. Yeon, B. C. Mohanty, Y. S. Cho, *ACS Appl. Mater. Interfaces* **2015**, *7*, 4573.

[32] Z. Chen, N. Prud'homme, B. Wang, V. Ji, *Surf. Coat. 80 [Eighty], Annu. Natl. Tech. Semin., 11th* **2011**, *206*, 405.

[33] M. Frelek-Kozak, L. Kurpaska, W. Pawlak, R. Diduszko, J. Jasinski, M. Chmielewski, J. Milczarek, J. Zoladek-Nowak, *J. Mol. Struct.* **2018**, *1166*, 34.

[34] Q. Zhou, D. He, Q. Zhuang, B. Liu, R. Li, H. Li, Z. Zhang, H. Yang, P. Zhao, Y. He, Z. Zang, J. Chen, *Adv. Funct. Mater.* **2022**, *32*, 2205507.

[35] Q. Zhou, J. Duan, X. Yang, Y. Duan, Q. Tang, *Angew. Chem.* **2020**, *132*, 22181.

[36] H. Guo, W. Xiang, Y. Fang, J. Li, Y. Lin, *Angew. Chem.* **2023**, *62*, 202304568.

[37] H. Xu, Y. Miao, N. Wei, H. Chen, Z. Qin, X. Liu, X. Wang, Y. Qi, T. Zhang, Y. Zhao, *Adv. Energy Mater.* **2022**, *12*, 2103151.

[38] Y. Zhao, F. Ma, Z. Qu, S. Yu, T. Shen, H.-X. Deng, X. Chu, X. Peng, Y. Yuan, X. Zhang, J. You, *Science* **2022**, *377*, 531.

[39] G. Kresse, J. Furthmüller, *Phys. Rev. B* **1996**, *54*, 11169.

[40] G. Kresse, D. Joubert, *Phys. Rev. B* **1999**, *59*, 1758.

[41] J. P. Perdew, K. Burke, M. Ernzerhof, *Phys. Rev. Lett.* **1996**, *77*, 3865.

[42] S. Grimme, J. Antony, S. Ehrlich, H. Krieg, *J. Chem. Phys.* **2010**, *132*.

[43] X. Lv, Z. Xu, J. Li, J. Chen, Q. Liu, *Appl. Surf. Sci.* **2016**, *376*, 97.